BNL-225110-2023-TECH

Nonlinear optics from hybrid dispersive orbits

Y. Li

December 2023

Photon Sciences

Brookhaven National Laboratory

U.S. Department of Energy

USDOE Office of Science (SC), Basic Energy Sciences (BES). Scientific User Facilities (SUF)

DISCLAIMER

NSLS-II TECHNICAL NOTE BROOKHAVEN NATIONAL LABORATORY	NUMBER **NSLSII-ASD-TN-397**
AUTHORS: Li, Y., Xu, D., Smaluk, V., Rainer, R.	DATE 12/20/2023
Nonlinear optics from hybrid dispersive orbits	

Nonlinear optics from hybrid dispersive orbits

Yongjun Li*, Derong Xu, Victor Smaluk, Robert Rainer
Brookhaven National Laboratory, Upton, New York 11973, USA

Abstract

In this paper we expand the technique of characterizing nonlinear optics from off-energy closed orbits (NOECO) to cover harmonic sextupoles in storage rings. The existing NOECO technique has been successfully used to correct the chromatic sextupole errors on the MAX-IV machine [Olsson et al., Phys. Rev. Accel. Beams **23**, 102803], however, it does not account for harmonic sextupoles, which are still widely used on many other machines. By generating vertical dispersion with chromatic skew quadrupoles, a measurable chromatic function dependence on harmonic sextupoles can be observed on hybrid dispersive orbits. Proof of concept of this technique was accomplished by simulations and beam measurements on the National Synchrotron Light Source II (NSLS-II) storage ring.

Keywords: Nonlinear lattice correction, chromatic and harmonic sextupoles

1. introduction

Characterizing the nonlinear optics of storage rings is becoming more essential with the introduction of higher order multipole magnets in accelerator design. Errors from nonlinear magnet strengths have been observed to degrade machine performance, such as reduction of dynamic aperture (DA) and local momentum aperture (LMA). Some efforts have been made to identify such errors by measuring local resonance [1] and distorted resonance driving terms [2], which

*Corresponding author
Email address: yli@bnl.gov (Yongjun Li)

requires a sophisticated Hamiltonian dynamics analysis. A more straightforward technique for measuring the nonlinear optics from off-energy closed orbits (NOECO) was reported and demonstrated on the MAX-IV ring [3]. Significant improvements on the DA and beam lifetime were observed after correcting sextupole errors. Some desired results were obtained while testing the NOECO technique on the ESRF-EBS ring as well [4]. However, the nonlinear chromatic functions on off-energy orbits is only measurable with chromatic sextupoles, where the horizontal dispersion is usually quite large, as to effectively correct the chromaticity. The existing technique, therefore, does not apply to harmonic sextupoles, which do not see the linear dispersion. Harmonic sextupoles are used in almost every third-generation light source ring, and some fourth-generation diffraction-limited machines, such as the ALS-U ring [5]. They are even being used in a future electron-ion collider ring [6]. As such, an expansion of the existing NOECO technique to correct harmonic sextupole errors would be useful due to their common, integral use in current and future accelerator design. In the National Synchrotron Light Source II (NSLS-II) ring [7], the number of harmonic sextupoles is much greater than that of chromatic sextupoles (180:90). Therefore, correcting harmonic sextupole errors is important for improving the machine performance.

A straightforward method for calibrating harmonic sextupoles for correction would be to temporarily convert them to chromatic ones. This could be achieved by tuning the quadrupoles inside achromats to generate a commensurate amount of dispersion at the locations of harmonic sextupoles [8]. However, this method would require a significant modification of the original linear lattice. Implementations during beam-based measurements, such as updating the nonlinear optics chromatic function for different leaked dispersion bumps would also be complicated. Another method would be to generate local orbit bumps through the sextupole calibration, and then measuring the optics distortion with different bump parameters. This method would not only require sufficient beam position monitors (BPMs) that neighbor the sextupoles, but would also be complicated to implement. For real-world applications, it is time-consuming

to form perfectly closed local bumps with orbit correctors, and then to update the chromatic optics on these bump settings [9]. While the above methods would be capable of achieving the desired outcome, they are not practical when considering the limitations of routine operations of user facilities.

In this paper we propose to account for harmonic sextupoles by generating vertical dispersion. When a normal sextupole sits on a vertical off-energy orbit $y_{co} = \eta_y \delta = \eta_y \frac{\Delta P}{P_0}$, its Hamiltonian reads as

$$H = \frac{p_x^2 + p_y^2}{2(1+\delta)} + \frac{K_2}{3}\left[x^3 - 3x\left(y + \eta_y \delta\right)^2\right]. \tag{1}$$

Here $p_{x,y}$ are the transverse momenta, and $K_2 = \frac{1}{(B\rho)_0}\frac{\partial^2 B_y}{\partial x^2}$ is the sextupole gradient. The Hamiltonian includes a skew quadrupole component $K_{1,s} = -2K_2\eta_y\delta$. Therefore, the coupled chromatic functions $\frac{d\beta}{d\delta}$ on this vertically displaced orbit depend on the sextupole gradient.

Vertical dispersion can be generated with chromatic skew quadrupoles. In most light source rings, skew quadrupoles are widely used to control residual vertical dispersion and linear coupling. Usually, a considerable amount of vertical dispersion can be generated, but only introduces a weak coupling when betatron tune is sufficiently isolated from resonances.

The remainder of this paper is outlined as follows: Sect. 2 introduces the principle of the technique in conjunction with the NSLS-II lattice. In Sect. 3 we demonstrate our technique with detailed simulations. A proof-of-principle beam measurement to calibrate both the chromatic and harmonic sextupole errors are given in Sect. 4, with the caveat that no real sextupole correction can be implemented at this time due to their in-series power supplies. Sect. 5 discusses the hardware requirements necessary to apply this technique. A brief summary is given in Sect. 6.

2. Nonlinear optics on hybrid dispersive orbit

In this section, the chromatic functions of the NSLS-II storage ring lattice were computed after vertical dispersion was generated. For this ring, each

odd-numbered cell is equipped with one 0.2 m long chromatic skew quadrupole (see Fig. 1). Their maximum gradients are $g_1 = \pm 0.35$ Tm^{-1}, limited by the capacity of their power supplies. Assuming we can double their gradients to $g_1 = \pm 0.70$ Tm^{-1}, a vertical dispersion wave with a ~ 0.1 m amplitude can be generated. The necessity for a double gradient will be discussed in Sect. 5. Although these gradients are twice as large as the maximum output of their existing power supplies, they are still quite weak compared to other operational quadrupoles with a maximum gradient of $g_{1,max} = \pm 22$ Tm^{-1}. Under these conditions, the exact coupled optics computed with the Ripken parameterization [10, 11] indicates that the linear optics remains weakly coupled. In Fig. 1, two non-dominating functions $\beta_{1,y}$ and $\beta_{2,x}$ (dashed lines) are observed as very close to zero, while the other two dominating $\beta_{1,x}$ and $\beta_{2,y}$ (solid lines) are almost the same as in the uncoupled case. The skew quadrupoles also cause a small amount of horizontal dispersion leakage into straight sections where harmonic sextupoles are located. Although such small leaked dispersion could not be solely used to measure the off-energy nonlinear optics, its effect is accounted for in our method because the exact optics parameterization is used. The newly generated vertical dispersion seen by the original harmonic sextupoles affect the nonlinear optics on off-energy orbits (as illustrated in Fig. 2) depending on their gradients. This dependence is utilized for the chromatic functions calibration and correction.

When horizontal dispersion is seen by sextupoles in an uncoupled linear optics configuration, the dependence of the chromatic β-function on the beam energy deviation δ, and the normalized sextupole gradient K_2, has been formulated [12]. When both horizontal and vertical dispersion can be seen by sextupoles, no such simple analytical formulae are available. However, it can be numerically computed with the two following methods. Method 1: First, for a given energy offset δ and skew quadrupole settings $K_{1,s}$, a hybrid dispersive closed orbit can be obtained with iterative tracking as implemented in many lattice codes, such as MAD-X [13] and ELEGANT [14]. Then a linear one-turn matrix R can be obtained along the dispersive orbit with the truncated power

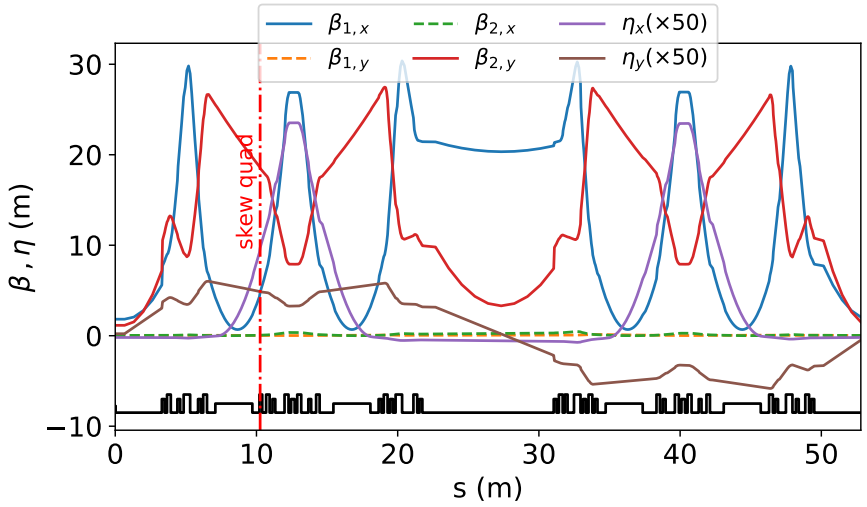

Figure 1: Exact Ripken Twiss functions for a supercell of NSLS-II when vertical dispersion is generated with chromatic skew quadrupoles (with a normalized gradient $K_{1,s} = \frac{1}{(B\rho)_0}\frac{\partial B_y}{\partial x} = 0.070\ \mathrm{m}^{-2}$). The location of the skew quadrupole is marked with a red vertical dash-dot line. The fact that $\beta_{2x,1y}$ (dashed lines) are small indicates that this optics remains weakly coupled.

series algorithm technique [15]. From the R matrix, four coupled Ripken Twiss functions can be extracted and propagated around the whole ring. By slightly tweaking the setting K_2 of a given sextupole and repeating the above procedure, the linear dependence of $\frac{d\beta}{d\delta}$ on its strength can be determined. Method 2: A direct particle tracking can be implemented with the same lattice setting as described in the previous method. When the initial particle coordinates are confined within the linear regime, the matrix R can also be fitted from multi-turn trajectories, then Ripken Twiss functions are obtained. Method 1, using the truncated series algorithm, was implemented with the MAD-X's PTC module [13], and method 2, using direct tracking, was carried out with the code ELEGANT. The consistency of two methods is illustrated in Fig. 3.

For demonstration purposes, we choose a harmonic sextupole, SH3, and a chromatic one, SM1, to compute the linear dependence of the chromatic func-

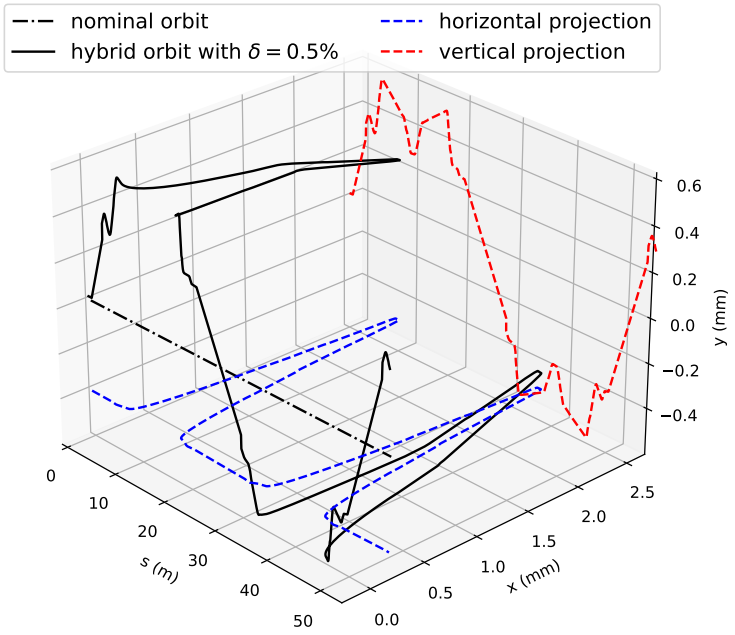

Figure 2: Three-dimensional view of the hybrid dispersive orbit with $\delta = 0.5\%$ for one NSLS-II supercell. For such orbits, harmonic sextupoles can see vertical displacements, then contribute to chromatic functions.

tions on their gradients. Only two dominating optics functions $\frac{d\beta_{1,x}}{d\delta}$ and $\frac{d\beta_{2,y}}{d\delta}$ were computed. The response vectors computed with the vertical dispersion, (denoted with "Y" in parentheses) and without the vertical dispersion, (denoted with "N") are compared in Fig. 4. On horizontal dispersive orbits, the dependence of off-energy optics on SH3 is not measurable in both the horizontal and vertical planes (blue lines). On hybrid dispersive orbits, a measurable dependence on SH3 can be observed (green lines). Note that, for both cases, the dependence on the chromatic sextupole, SM1, is always measurable because it always sees a large horizontal dispersion. In both cases, the dependencies on SM1 remain almost unchanged since the optics is only slightly altered.

In principle, chromatic and harmonic sextupole errors can be calibrated simultaneously with a sufficiently large vertical dispersion. However, chromatic

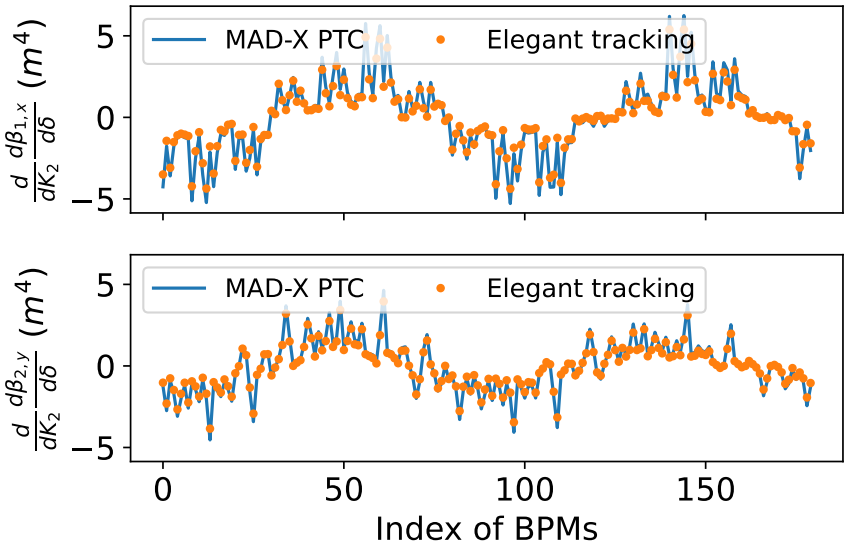

Figure 3: Comparison of the chromatics optics dependence on one harmonic sextupole computed with two different methods/codes. The results obtained were consistent with each other. The blue lines were computed with the code MAD-X's PTC module. The orange dots were from direct tracking using the code ELEGANT. The top subplot is the response vector in the horizontal plane. The bottom one is in the vertical plane.

sextupoles usually have stronger responses than harmonic ones, as the vertical dispersion obtained through coupling is smaller than the horizontal one. Therefore, for practical purposes, we can uncouple the chromatic and harmonic sextupole correction via a two-stage correction. Stage 1: correcting chromatic sextupoles first with the existing technique [3]. Stage 2: generating a vertical dispersion wave, then calibrating harmonic sextupoles from hybrid dispersive orbits. In this paper, we mainly focus on the 2^{nd} stage because the 1^{st} stage has already been well studied with the linear optics from closed orbits (LOCO) algorithm [16] in the ref. [3].

The β-functions and phase advances can be measured directly from turn-by-turn (TBT) data using Fourier analysis [17], or the numerical analysis of fundamental frequencies (NAFF) algorithm [18, 19]. Therefore, instead of the

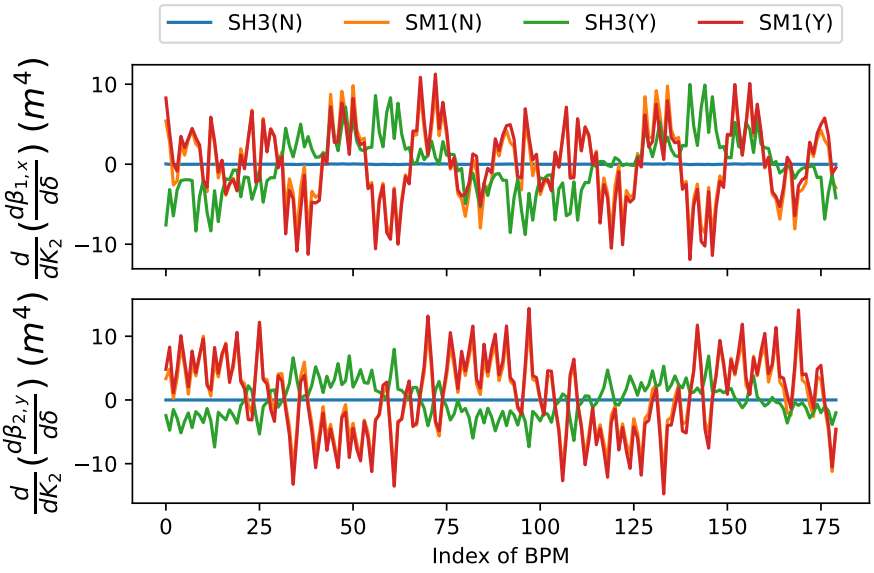

Figure 4: Comparison of the off-energy optics dependence on a chromatic sextupole SM1 and a harmonic sextupole SH3. On horizontal dispersive orbits, the optics dependence on the harmonic sextupole (blue lines labeled as SH3(N)) is too small to measure. On hybrid dispersive orbits, a measurable dependence (green lines labeled as SH3(Y)) is observed.

LOCO algorithm, the TBT analysis was used here. We first used the NAFF technique to compute the Fourier component amplitude A of the spectral lines associated with two eigen-tunes, which is proportional to the square root of the β-functions, at each BPM location, and on each transverse plane.

$$A_{(1,2),(x,y)} = \sqrt{J_{(1,2)}\beta_{(1,2),(x,y)}} \tag{2}$$

where $J_{1,2}$ are the linear actions for two coupled modes and depend on the initial excitations. Then the TBT data from two neigboring BPMs with only a linear drift in-between was used to reconstruct their linear one-turn maps M. Here the conjugate momenta were obtained with following equations,

$$p_x \approx x' = \frac{x_d - x_u}{L},\ p_y \approx y' = \frac{y_d - y_u}{L}, \tag{3}$$

where the subscript u represents the upstream BPM, d for the downstream one, and L is the distance in-between. Next, the coupled β-functions at these

two BPMs were extracted with the Ripken parameterization of M's. Thus the actions $J_{(1,2)}$ were calibrated as $J = \frac{A_{u,d}^2}{\beta_{u,d}}$ and used to normalized the rest of the BPMs to estimate their absolute β-functions.

Given a vertical dispersion pattern as shown in Fig. 1, the response matrices (RM) of $\frac{d\beta_{(1,x),(2,y)}}{d\delta}$ dependence on 180 harmonic sextupoles were computed with the lattice model. $\beta_{(1,y),(2,x)}$ were ignored because they are too small to be measured accurately. The results of response matrix computation are shown in Fig. 5.

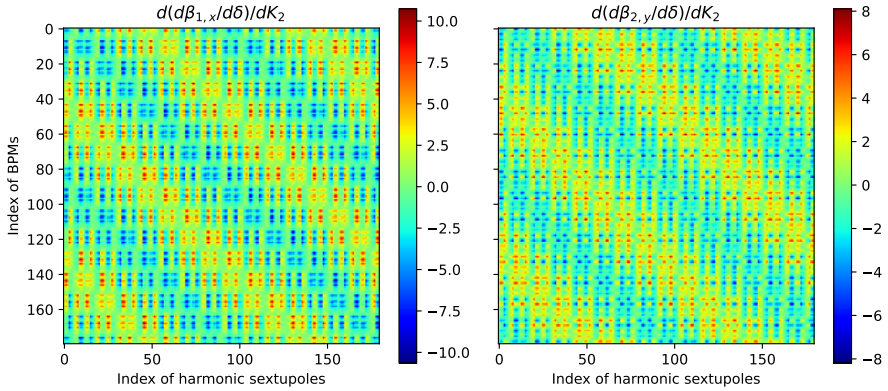

Figure 5: Given a hybrid dispersion wave in Fig. 1, the harmonic sextupole response matrices (RM) observed at the BPMs are obtained by computing the deviation of $\frac{d\beta}{d\delta}$ while tweaking each individual harmonic sextupole from its nominal setting. Left: the $\beta_{1,x}$ function's RM in the horizontal plane. Right: the $\beta_{2,y}$ function's RM in the vertical plane.

3. Simulations

Below we simulated two specific cases to study the performance expectation of this correction technique.

3.1. Case 1: two individual isolated errors

First, we studied a case in which two isolated (far apart from each other) sextupoles errors $\Delta K_2 = +1.5,\ -1\ \mathrm{m}^{-3}$ were added onto the 32^{th}, 154^{th} harmonic sextupoles. The corresponding relative errors are $\frac{\Delta K_2}{K_2} \sim 5 - 6\%$. The

distortions $\Delta\frac{d\beta}{d\delta}$ observed at the BPMs are shown with the dashed lines in Fig. 6. The needed corrections $-\Delta K_2$ were obtained by solving the following linear regression problem with the response matrices computed in the previous section,

$$\Delta\frac{d\beta}{d\delta} = \left(\frac{d\beta}{d\delta}\right)_{error} - \left(\frac{d\beta}{d\delta}\right)_{model} \approx M_{x,y}\Delta K_2, \tag{4}$$

here, $\left(\frac{d\beta}{d\delta}\right)_{model}$ are the ideal chromatic functions, $\left(\frac{d\beta}{d\delta}\right)_{error}$ are the distortions due to the given errors, and $M_{x,y}$ are the vertically stacked horizontal (M_x) and vertical (M_y) response matrices in Fig. 5.

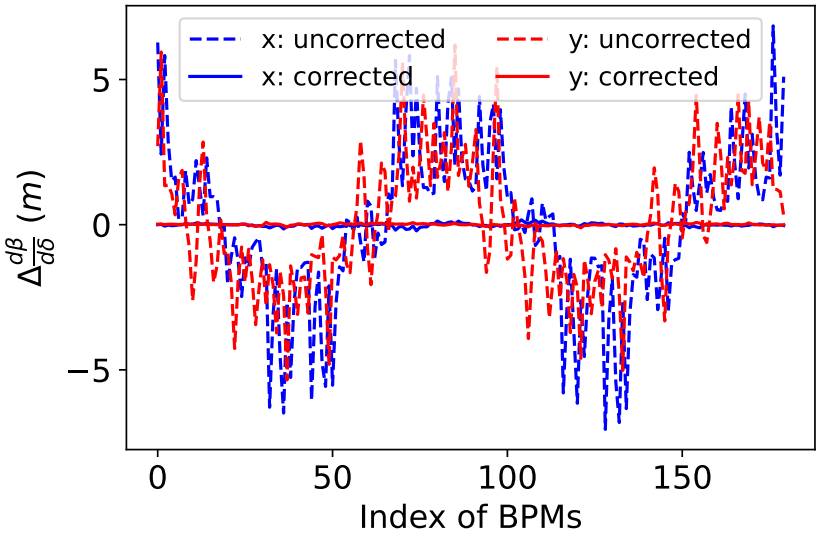

Figure 6: Comparison of nonlinear optics distortions, before and after correction, in the presence of two isolated sextupole errors. The dashed lines are the uncorrected distortions, and the solid lines represent the corrected ones.

The correction scheme obtained with Eq. (4) is shown in Fig. 7. Due to the high degeneracy among the neighboring sextupoles, the scheme does not reproduce the original specified errors. Instead, they spread to their neighbors. Nevertheless, the errors were localized, and after applying the correction scheme, the nonlinear optics was improved as illustrated in Fig. 6.

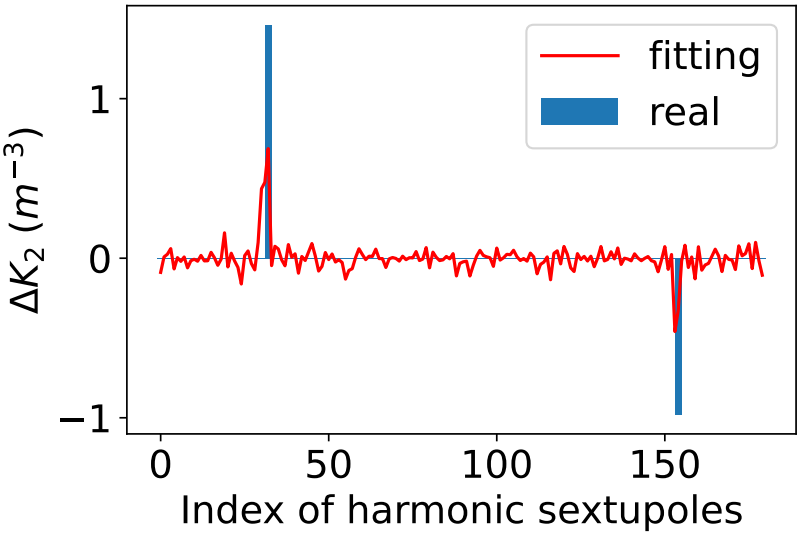

Figure 7: Correction scheme for two isolated sextupole errors, obtained by the linear regression algorithm. Despite high degeneracy among sextupoles, two error sources are localized, and chromatic function distortions were well corrected.

3.2. Case 2: normally distributed errors

In this case, randomly distributed errors $\left(\frac{\Delta K_2}{K_2}\right)_{rms} \sim 7\%$ on all 180 harmonic sextupoles were introduced and the distortion of off-energy optics were computed. Then the same correction procedure was employed. The optics distortions before and after correction, and the real error distributions and computed corrections are illustrated in Fig. 8 and Fig. 9, respectively.

To simulate the imperfections of BPMs, 10 µm (the NSLS-II BPMs' TBT resolution after calibration [20]) random errors were added on the TBT data for this case. Similar to the previous cases, the obtained corrections only approximately follow the real, pre-specified error distributions. This is due to the strong degeneracy that exists among sextupoles in the NSLS-II lattice. However, the distortion of nonlinear optics can still be significantly improved in Fig. 8. Comparing with the previous case in which the BPMs were assumed to be perfect, the correction performance now became lower with BPM errors. Therefore,

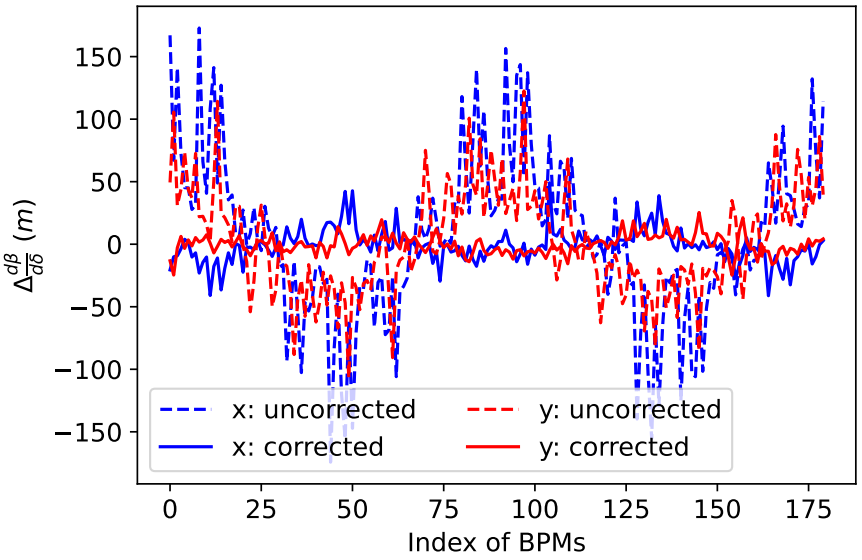

Figure 8: Distortions of the nonlinear optics with randomly added errors on 180 harmonic sextupoles. The dashed lines are uncorrected distortions, and the solid lines represent the corrected distortions. The imperfection of BPMs are considered in this case.

a high resolution BPM system is desired for this technique. It is also worth mentioning that the dependence of chromatic optics on sextupoles is nonlinear, therefore, an iterative correction might be necessary in online measurements.

3.3. Improvement on dynamic aperture degradation

As observed in the previous simulations, strong degeneracy among sextupoles prevents reproducing the pre-specified error distributions. It is because, on the NSLS-II ring, every three harmonic sextupoles on the same girder were closely assembled. In this case, what is actually corrected is the first-order nonlinear chromatic optics distortion seen by the BPMs. The correction scheme based on the BPM observations, therefore, is only able to recover the nonlinear optics rather than DA. However, we believe that the DA and LMA should be improved to some extent after the distorted chromatic functions were corrected. To illustrate this, the on- and off-momentum DAs of the ideal machine, uncorrected

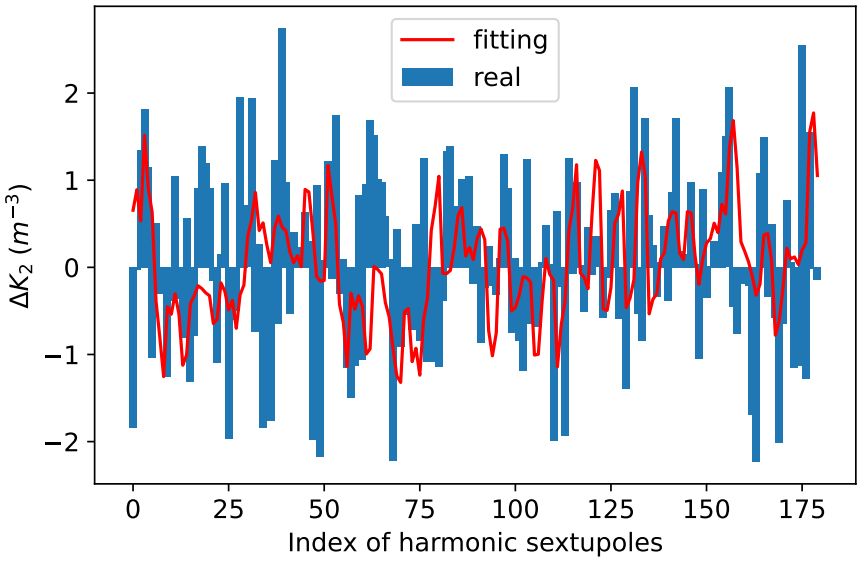

Figure 9: Comparison of the added errors (labeled as "real") on 180 harmonic sextupoles and the obtained correction scheme (shown with red lines labeled as "fitting").

and corrected nonlinear lattices for the 2^{nd} simulation were computed as shown in Fig. 10. It was observed that, although the degraded DA due to sextupole errors could not be fully recovered through the linear correction scheme Eq. (4), a modest improvement was actually achieved. Such improvements on DA and LMA are the main purpose of calibrating and correcting the distorted nonlinear optics. If we could distinguish between the degeneracy among the sextupoles, further improvement should be expected. This topic was investigated [21] and is worth further study.

4. Two-stage measurements

As NSLS-II sextupoles are powered in series, they lack individual configurability. No actual nonlinear optics correction can be implemented with these limitations. However, a two-stage proof-of-principle, using beam-based calibration of chromatic functions was implemented, and a correction scheme was

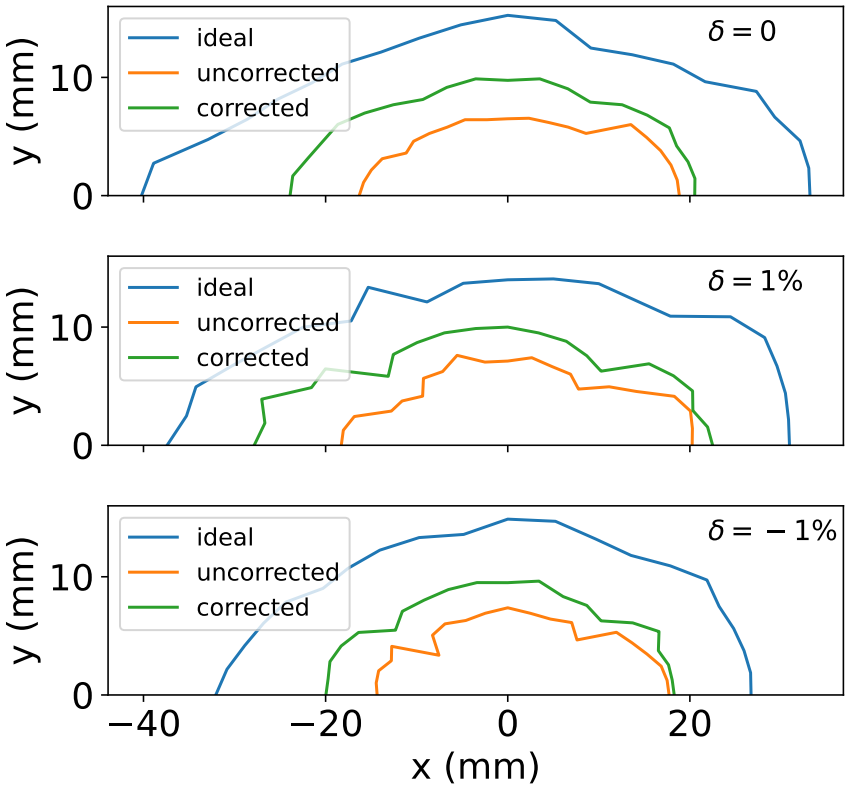

Figure 10: Results of the on- and off-momentum DAs for the ideal machine, uncorrected and corrected nonlinear lattices. Although the degraded DA (yellow lines) could not be well recovered to that of the ideal machine (blue lines), modest improvements (green lines) were achieved, through correcting the first order distorted nonlinear optics.

proposed. At stage 1, we calibrated 90 chromatic sextupoles with similar techniques as used in ref. [3]. First, the linear optics were well corrected (with a 1–2% residual β-beat). Then, spurious vertical dispersion was minimized using 15 chromatic skew quadrupoles, and the global linear coupling was minimized with another 15 non-dispersive skew quadrupoles. The purpose of minimizing spurious vertical dispersion and linear coupling is to mitigate the residual hybrid dispersive orbit created by random skew quadrupole components. At NSLS-II, the gain and roll errors in each BPM have been calibrated before.

The β-functions measured with calibrated TBT readings have a 0.03 m resolution. The $\frac{d\beta}{d\delta}$ seen by the BPMs were measured from horizontal dispersive orbits through varying beam energies within $\delta \in [-0.27\%, 0.27\%]$ by changing the main RF oscillator frequency within $\Delta f \in [500, -500] Hz$. By comparing the measured nonlinear optics against the design model $\left(\frac{d\beta}{d\delta}\right)_{meas.} - \left(\frac{d\beta}{d\delta}\right)_{model}$ (Fig. 11: top), the chromatic sextupole corrections (red bars in Fig. 13) were obtained with Eq. (4) using the ideal model response matrices (Fig. 5). Since individual chromatic sextupole correction could not be implemented, we incorporated this sextupole correction scheme into the lattice model to update the reference optics, and their corresponding response matrices as well. In this way, at the next stage, the chromatic sextupole errors were included in the updated model/matrices, and would not affect the calibration of harmonic sextupoles.

For stage 2, a vertical dispersion wave was generated with 15 dispersive skew quadrupoles to their maximum capacity. Based on the measured dispersion, the 15 skew quadrupole settings and the vertical dispersion at the BPMs were reproduced with the lattice model as illustrated in Fig. 12. To achieve greater accuracy, a large amplitude vertical dispersion wave is preferred. However, it is limited by the capacity of the skew quadrupole power supplies. Under the current configuration, ~ 0.05 m is the maximum amplitude that can be generated. The $\frac{d\beta}{d\delta}$ seen by the BPMs were re-measured, but from hybrid dispersive orbits this time (Fig. 11: bottom). With the updated lattice model (incorporated with skew quadrupoles and chromatic sextupole errors) as the new reference, a 180 harmonic sextupole correction scheme was obtained (blue bars in Fig. 13). As explained previously, Fig. 13 only represents a proposed sextupole correction scheme to reduce the distortion of nonlinear optics, and does not need to be the actual error distributions.

Since skew quadrupoles are used as corrector magnets on our machine, their hysteresis was found to be negligible. After tuning them to generate vertical dispersion and then restoring their nominal settings, no visible residual effects on the injection efficiency and beam lifetime were observed. Therefore, this technique can be used as a practical method for routine operation of user facil-

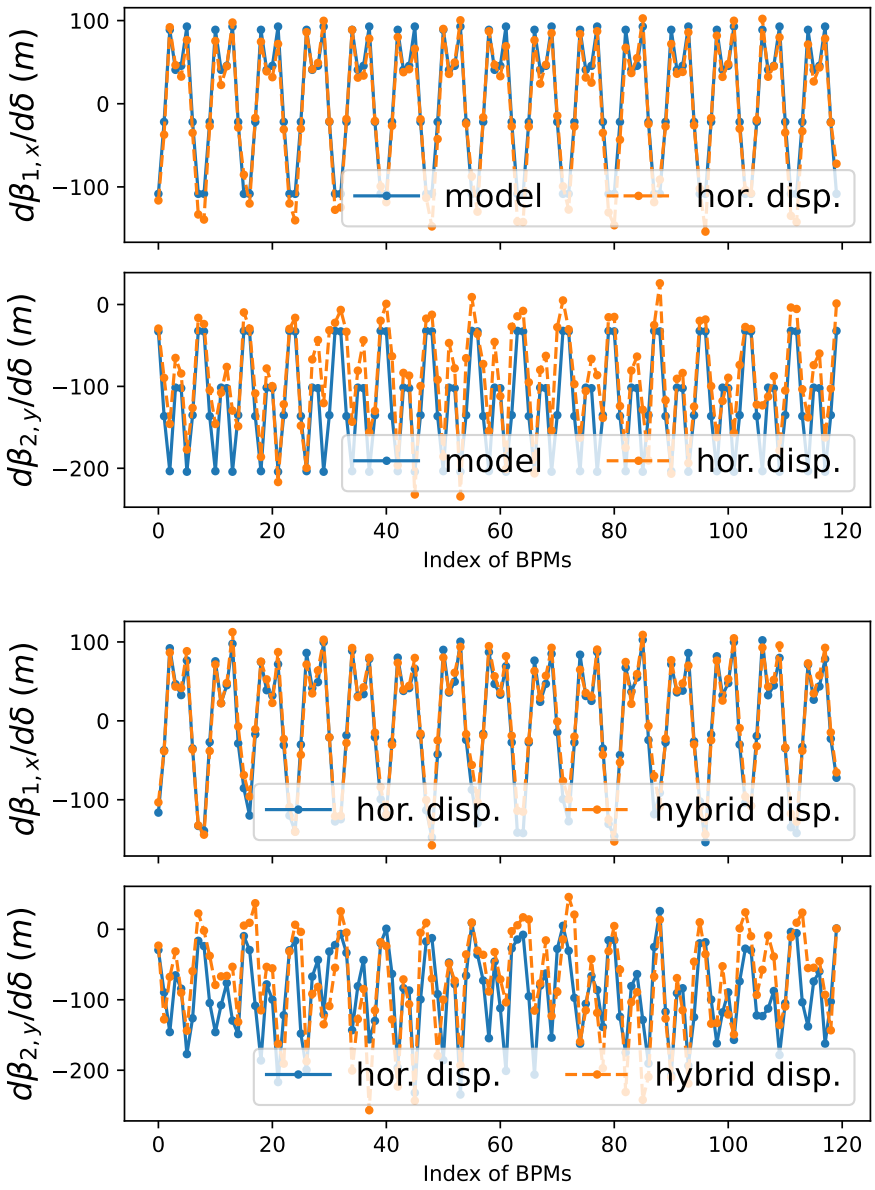

Figure 11: Measured off-energy optics at two stages. Top: chromatic optics of the ideal model and online measurements from horizontal dispersive orbits which were used to calibrate the chromatic sextupoles. Bottom: beam-based measurements of off-energy optics from hybrid dispersive orbits, which were used to calibrate the harmonic sextupoles.

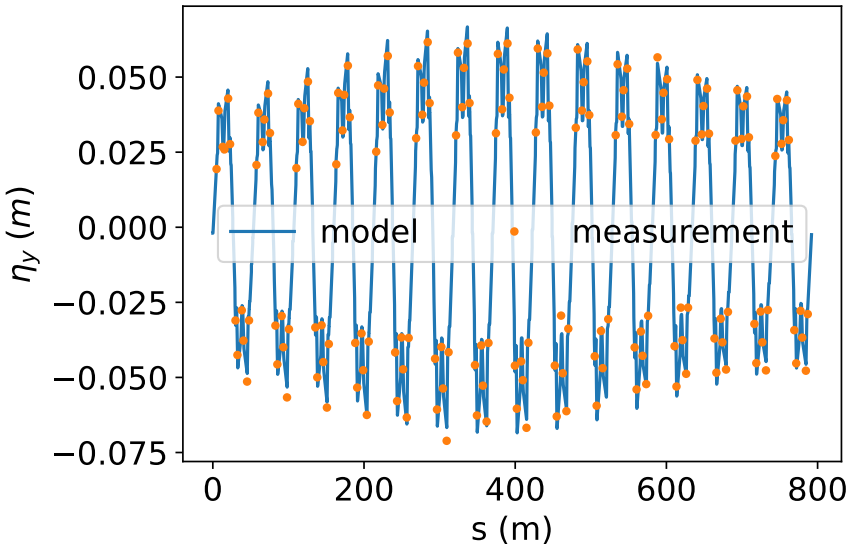

Figure 12: Measured vertical dispersion seen by the BPMs, and its reproduction with the lattice model.

ities.

5. Requirements on power supplies of magnets

In the previous section, we saw the measurements at NSLS-II were limited by hardware. Here, we specify the requirements of the power supplies for the skew quadrupoles and sextupoles to make this calibration and correction practical. First, sextupoles need to be powered independently, or equipped with back-leg windings to allow individual tunability. Second, the skew quadrupoles that generate the vertical dispersion wave should be sufficiently strong for better resolution.

Below we estimate the desired skew strengths for the NSLS-II lattice. The resolution of the β-function measurement using turn-by-turn data was found at a level of about 0.03 m on our storage ring. Assuming we adjust the RF frequency by $\pm 1,000$ Hz, the corresponding energy deviation is $\Delta\delta = -\frac{1}{\alpha_c}\frac{\Delta f}{f_0} \approx 1.0\%$ with

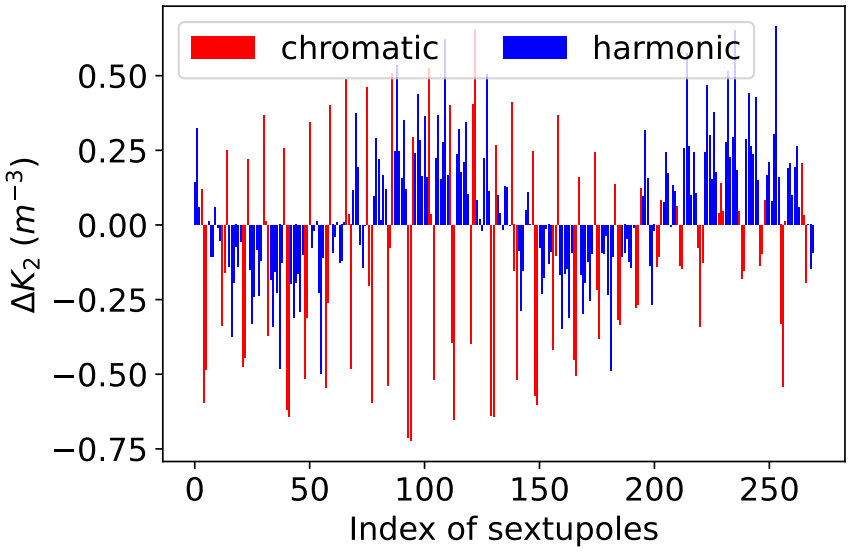

Figure 13: A proposed sextupole correction scheme from the two-stage measurements. The chromatic sextupoles marked with red bars are from the first stage, while the harmonic ones (blue bars) are from the second stage.

α_c momentum compaction factor. To resolve a single harmonic sextupole error to the level of 1 unit $\Delta K_2 = 1$ m^{-3}, the magnitude of $\frac{d}{dK_2}\frac{d\beta}{d\delta}$ needs to be greater than 3 m^4. To generate such a strong dependence, the amplitude of the vertical dispersion wave is required to be greater than 0.1 m. In order to couple 0.1 m dispersion to the vertical plane, a $K_{1,s} \geq 0.070$ m^{-2} is needed to apply to all 15 skew quadrupoles. Therefore, strong skew quadrupoles were chosen to identify chromatic function errors in our simulations. Although a $g = \frac{\partial B_x}{\partial x} = (B\rho)_0 K_{1,s} = 0.70$ Tm^{-1} quadrupolar gradient is quite weak, it actually exceeds the capacity of our existing skew quadrupole power supplies, which can only provide $g_{2,max} = 0.35$ Tm^{-1}. In other words, stronger skew quadrupoles are needed to generate larger vertical dispersion for better resolution. In our measurements, as all sextupoles have some associated errors, the accumulated magnitude of $\Delta\frac{d\beta}{d\delta}$ are at the level of 100–200 meters, which allows us to calibrate the approximate error distributions. However, these have low accuracy as shown

in the Sect. 4.

The above estimation does not consider even higher orders of nonlinear optics from off-energy orbits. Once the higher order nonlinearities $\frac{d^n\beta}{d\delta^n}$ with $n \geq 2$ appear, we could not improve the measurement accuracy by simply increasing beam energy offsets. On the other hand, increasing skew quadrupole strengths to generate higher vertical dispersive orbits can significantly improve the sensitivity of off-energy optics to sextupole settings without introducing too much linear coupling and nonlinearity. Therefore, having sufficiently strong skew quadrupoles should be considered a necessary condition for this technique.

6. Summary

In our investigation, we expanded the capabilities of the technique for measuring nonlinear optics distortions from off-energy closed orbits to account for the harmonic sextupole contribution. From distorted chromatic functions on hybrid dispersive closed orbits, the corrections of the harmonic sextupoles can be obtained. A practical benefit of our expanded method is that a considerable amount of vertical dispersion can be generated with weak skew quadrupoles. Meanwhile, because the lattice is only weakly coupled, its optics properties can still be well maintained. In our studies, only the sextupole correction was considered. As for higher order, nonlinear magnets, such as octupoles, we have not yet investigated. This technique may be applicable if their dependencies to the first order chromatic functions were sufficiently strong.

Acknowledgements

We would like to thank Dr. D. Olsson (MAX IV, Lund Uni.), Prof. Y. Hao (MSU), and some NSLS-II colleagues, Dr. J. Choi, Dr. Y. Hidaka, Dr. M. Song, Dr. G. Tiwari, Dr. X. Yang et al., for the collaborative and productive discussion that went into this investigation. This research used resources of the National Synchrotron Light Source II, a U.S. Department of Energy (DOE) Office of

Science User Facility operated for the DOE Office of Science by Brookhaven National Laboratory under Contract No. DE-SC0012704.

References

[1] R. Bartolini, I. Martin, J. Rowland, P. Kuske, F. Schmidt, Correction of multiple nonlinear resonances in storage rings, Physical Review Special Topics-Accelerators and Beams 11 (10) (2008) 104002.

[2] A. Franchi, L. Farvacque, F. Ewald, G. Le Bec, K. Scheidt, First simultaneous measurement of sextupolar and octupolar resonance driving terms in a circular accelerator from turn-by-turn beam position monitor data, Physical Review Special Topics-Accelerators and Beams 17 (7) (2014) 074001.

[3] D. Olsson, Å. Andersson, M. Sjöström, Nonlinear optics from off-energy closed orbits, Physical Review Accelerators and Beams 23 (10) (2020) 102803.

[4] S. Liuzzo, N. Carmignani, L. Carver, L. Hoummi, T. Perron, B. Roche, S. White, Lifetime correction using fast-off-energy response matrix measurements, in: 13th International Particle Accelerator Conference, 2022, p. TUPOMS008.

[5] C. Sun, H. Nishimura, D. Robin, F. Sannibale, C. Steier, M. Venturini, W. Wan, Optimization of the ALS-U Storage Ring Lattice, in: 7th International Particle Accelerator Conference, 2016, p. WEPOW050. doi:10.18429/JACoW-IPAC2016-WEPOW050.

[6] Y. Cai, Y. Nosochkov, S. Berg, J. Kewisch, Y. Li, D. Marx, C. Montag, S. Tepikian, F. Willeke, G. Hoffstaetter, et al., Optimization of chromatic optics in the electron storage ring of the electron-ion collider, Physical Review Accelerators and Beams 25 (7) (2022) 071001.

[7] S. Dierker, et al., NSLS-II preliminary design report, Tech. rep., Brookhaven National Lab, Upton, NY, USA (2007).

[8] D. Olsson, personal communication.

[9] J. Choi, personal communication.

[10] I. Borchardt, E. Karantzoulis, H. Mais, G. Ripken, Calculation of beam envelopes in storage rings and transport systems in the presence of transverse space charge effects and coupling, Zeitschrift für Physik C Particles and Fields 39 (3) (1988) 339–349.

[11] F. Willeke, G. Ripken, Methods of beam optics, in: AIP Conference Proceedings, Vol. 184, American Institute of Physics, 1989, pp. 758–819.

[12] H. Wiedemann, Particle accelerator physics, 3rd Edition, Springer, 2007.

[13] F. Schmidt, MAD-X PTC integration, in: Proceedings of the 2005 Particle Accelerator Conference, IEEE, 2005, pp. 1272–1274.

[14] M. Borland, elegant: A flexible SDDS-compliant code for accelerator simulation, Advanced Photon Source, LS-287.

[15] A. Berz, Differential algebraic description of beam dynamics to very high orders, Part. Accel. 24 (SSC-152) (1988) 109–124.

[16] J. Safranek, Experimental determination of storage ring optics using orbit response measurements, Nuclear Instruments and Methods in Physics Research Section A: Accelerators, Spectrometers, Detectors and Associated Equipment 388 (1-2) (1997) 27–36.

[17] J. Borer, C. Bovet, A. Burns, G. Morpurgo, Harmonic analysis of coherent bunch oscillations in LEP, Conf. Proc. C, 3rd European Particle Accelerator Conference (EPAC 92) 920324 (1992) 1082–1084.

[18] J. Laskar, C. Froeschlé, A. Celletti, The measure of chaos by the numerical analysis of the fundamental frequencies. application to the standard mapping, Physica D: Nonlinear Phenomena 56 (2-3) (1992) 253–269.

[19] P. Zisopoulos, Y. Papaphilippou, A. Streun, V. Ziemann, Beam Optics Measurements through Turn by turn Beam Position Data in the SLS, in: 4th International Particle Accelerator Conference, 2013, p. WEPEA067.

[20] Y. Hao, Y. Li, M. Balcewicz, L. Neufcourt, W. Cheng, Reconstruction of storage ring's linear optics with bayesian inference, arXiv preprint arXiv:1902.11157.

[21] D. Vilsmeier, R. Singh, M. Bai, Inverse modeling of circular lattices via orbit response measurements in the presence of degeneracy, Physical Review Accelerators and Beams 26 (3) (2023) 032803.